Available online at www.sciencedirect.com
ScienceDirect
Journal of Power Sources 164 (2007) 822–828
JOURNAL OF POWER SOURCES
www.elsevier.com/locate/jpowsour

Synthesizing kinetics and characteristics for spinel $LiMn_2O_4$ with the precursor using as lithium-ion battery cathode material

Ming Shu Zhao *, Xiao Ping Song

Materials Physics & Chemistry, Science School, Xi'an Jiaotong University, 710049 Xi'an, China

Available online 14 December 2006

Abstract

The discomposing kinetics of lithium manganese oxides precursor in dynamical air atmosphere was studied by means of DTA with different heating rates, and it could be applied as an important theoretical principle for preparing $LiMn_2O_4$. The active energies of four reaction processes were obtained with Doyle–Ozawa method and Kissinger method as follows: 69.831, 165.093, 326.128, and 645.983 kJ mol^{-1}, respectively. Reaction orders, frequency factors and kinetic equations of each reaction were determined by using Kissinger method. XRD, SEM and TEM showed that the synthesized $LiMn_2O_4$ using the precursor is a pure phase, with regular appearance and higher ratio-surface.

Keywords: Lithium-ion battery; $LiMn_2O_4$; Precursor; Kinetics

1. Introduction

Lithium-ion cells, the third generation rechargeable green batteries after nickel–cadmium cells and nickel–hydrogen cells, are used widely in the field of mobile phone, digital camera, portable computer, and the other modern electronic equipments by virtues of lower self-resistance, little self-discharge, high ratio energy, without memorizing effect and pollution [1,2]. It is estimated that the output of lithium-ion cells could reach to 5–6 billions with exceeding $50 billion total sales in 2003, displaying the excellent market prospect [3,4].

The researches show that the properties for lithium-ion battery cathode materials are affected by materials selection, chemical proportion and controllable conditions during the experimental course [5,6]. Using co-precipitation method, the advantages of synthesizing spinel $LiMn_2O_4$ are the evenly compositions of precipitation within atom size order, overcoming the disadvantages of long-cycle and high-energy exhausting with solid-phase method, and lowering synthesis cost. Moreover, the product has well-scattered particle, regular appearance, and developed crystal phase [7].

Up to now, the dynamic study of synthesizing lithium–manganese compounds precursor has not been reported in detail. The dynamic parameters could be as theoretical principles for preparing lithium–manganese compounds. By means of differential thermal analyzer, kinetics values of reaction active energy, reaction order number and frequency factor for each react stage in the process of synthesizing lithium manganese in dynamic air atmosphere were calculated. So the velocity equation could be induced. The corresponding relationships between temperature difference of sample-reference and temperature were detected at procedural controlling temperature. There are four different differential thermal analyzer curves measured at different heating rates in order to overcome some shortcomings such as deviation temperature of sample between thermal results and procedures, temperature gradient existing external sample [8,9].

2. Experimental

The molar ratio of $LiNO_3$ (analyze pure) and $Mn(NO_3)_2 \cdot 6H_2O$ (analyze pure) was 1.1:1 and the reactant solution for $LiNO_3$ and $Mn(NO_3)_2 \cdot 6H_2O$ whose concentration were both 1 mol L^{-1} were mixed. During the reaction course, the constant temperature of water bath was 25 °C and the $Na_2CO_3 \cdot 10H_2O$ solution was dropped until pH value of the admixture solution was 10.90. During the ageing course, the constant temperature was 60 °C, ageing time was 5 h. The lithium manganese oxide precursor powder, obtained after filtration, washing and desiccation, was ground, pressed and put into a corundum boat, then placed at Fe–Cr–Al wire horizontal furnace. The heating temperature was 650 °C controlled by

* Corresponding author. Tel.: +86 29 82665471; fax: +86 29 82667872.
E-mail address: zhaomshu@mail.xjtu.edu.cn (M.S. Zhao).

0378-7753/$ – see front matter © 2006 Elsevier B.V. All rights reserved.
doi:10.1016/j.jpowsour.2006.11.001

Nomenclature

A	Frequency factor (s^{-1})
E	active energy ($J\,mol^{-1}$)
n	reaction order
r	linear regression correlation coefficient
R	gas constant (8.314 $J\,mol^{-1}\,K^{-1}$)
t	time (s)
T	temperature (K)

Greek symbols

α	fractional conversion (%)
β	heating rate ($K\,min^{-1}$)

WZK type governing silicon temperature apparatus utilizing nickel–chromium/nickel–silicon thermocouple. After the reaction finished, the furnace was cooled to room temperature, and the sample was taken from the furnace.

The precursor weighting 13.54 mg (±0.05 mg) was put into a 150 μl platinum crucible. The DTA experiments under different heating rates, which was 8, 10, 15 and 20 K min^{-1}, respectively, were done at ~25 mL min^{-1} flux of dynamic air atmosphere with PERKIN-ELMER 7 Series analysis system.

According to the measured DTA curves, the precursor carbonate oxide lithium manganese is thermostatic at 653, 803 or 1053 K for 30 min, respectively, and cooled quickly, then the obtained substance was analyzed by using RIGAKU/MAC-3B type X-ray diffraction instrument, applying Ni-filter and Cu Kα (50 mA). The scanning rate and step of the half width value were 10 °C min^{-1} and 0.02°, separately. The grading analysis of the sample was tested using Malvern granulometer. The surface of the sample was coated with a layer gold film using JFC-1100E type ion-sputtering device whose vacuum degree is 10^{-6} Pa. The handled sample was observed by using JSM-5800 type scanning electron microscope. The sample was well dispersed in the solution of some certain solvent, and was caught with the micro-copper-mesh, then was observed by using H-600 type transmission electron microscope.

3. Results and discussion

3.1. Decomposition of lithium manganese oxide precursor

The experiments were conducted at dynamic air flux of ~25 mL min^{-1} with different heating rates of 8, 10, 15 and 20 K min^{-1}. The loss weight, peak temperature, heating flow rates, enthalpy variation and peak areas of each endothermic peak or exothermic peak could be tested under different heating rates. The DTA curves of carbonate oxide lithium manganese were given in Fig. 1. According to the measurement zero line, it could be seen from the Fig. 1 that there were four peaks including two endothermic peaks, and two exothermic peaks. The first endothermic peak appeared within temperature scope of 593–653 K and the first exothermic peak whose shape was narrow emerging within temperature limit of 753–803 K. Between

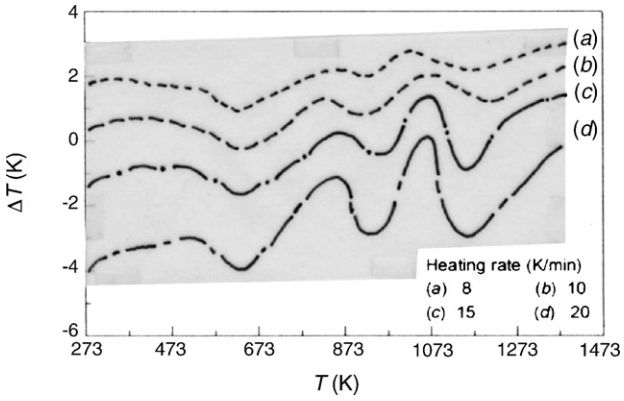

Fig. 1. The DTA curves of carbonate oxide lithium manganese.

873 and 973 K, there existed the second exothermic peak, which was a long distance peak shape. During the temperature course of 1073–1173 K, the second endothermic peak appeared, showing that lithium manganese oxide started to decompose.

Under the appropriate experimental conditions, each composition of precursor reacted as following:

$$LiNO_3 + Na_2CO_3{\cdot}10H_2O \rightarrow Li_4O(CO_3){\cdot}H_2O \downarrow + NaNO_3 + H_2CO_3 \quad (1)$$

$$Mn(NO_3)_2{\cdot}6H_2O + Na_2CO_3{\cdot}10H_2O \rightarrow Mn_2OCO_3{\cdot}H_2O \downarrow + NaNO_3 + H_2CO_3 \quad (2)$$

During the precipitation process, reactions (1) and (2) occurred simultaneously, thus, the precursor $(Li_2Mn_4)O(CO_3)_4{\cdot}H_2O$ was formed. So the assemble reaction could be written as following:

$$LiNO_3 + Mn(NO_3)_2{\cdot}6H_2O + Na_2CO_3{\cdot}10H_2O \rightarrow (Li_2Mn_4)O(CO_3)_4{\cdot}H_2O \downarrow + NaNO_3 + H_2CO_3 \quad (3)$$

The X-ray diffraction patterns of precursor powder heated at 653, 803 or 1053 K were showed in Fig. 2. It could be seen from Fig. 2(a) that the sample was still carbonate oxide lithium manganese. It was obvious that the first peak of DTA curve was caused by de-hydrolysis endothermic for the precursor. By calculating weight loss, the dehydration number is 1. Thus, the first endothermic peak of DTA curve is de-hydrolysis reaction. Similarly, we know that the second peak of precursor decomposition was de-carbon producing gas phase. During the sintering course, the involving reactions for precursor were the following:

$$(Li_2Mn_4)O(CO_3)_4{\cdot}H_2O \rightarrow (Li_2Mn_4)O(CO_3)_4 + H_2O \uparrow \quad (4)$$

$$(Li_2Mn_4)O(CO_3)_4 + O_2 \rightarrow LiMn_2O_4 + CO_2\uparrow + CO \uparrow \quad (5)$$

$$(Li_2Mn_4)O(CO_3)_4 + O_2 \rightarrow LiMn_2O_4 + CO_2 \quad (6)$$

3.2. Kinetics principle

From the viewpoints of chemistry reaction dynamics, the variations of chemical reaction velocity with time, concentration and temperature were studied, and the dynamic equations

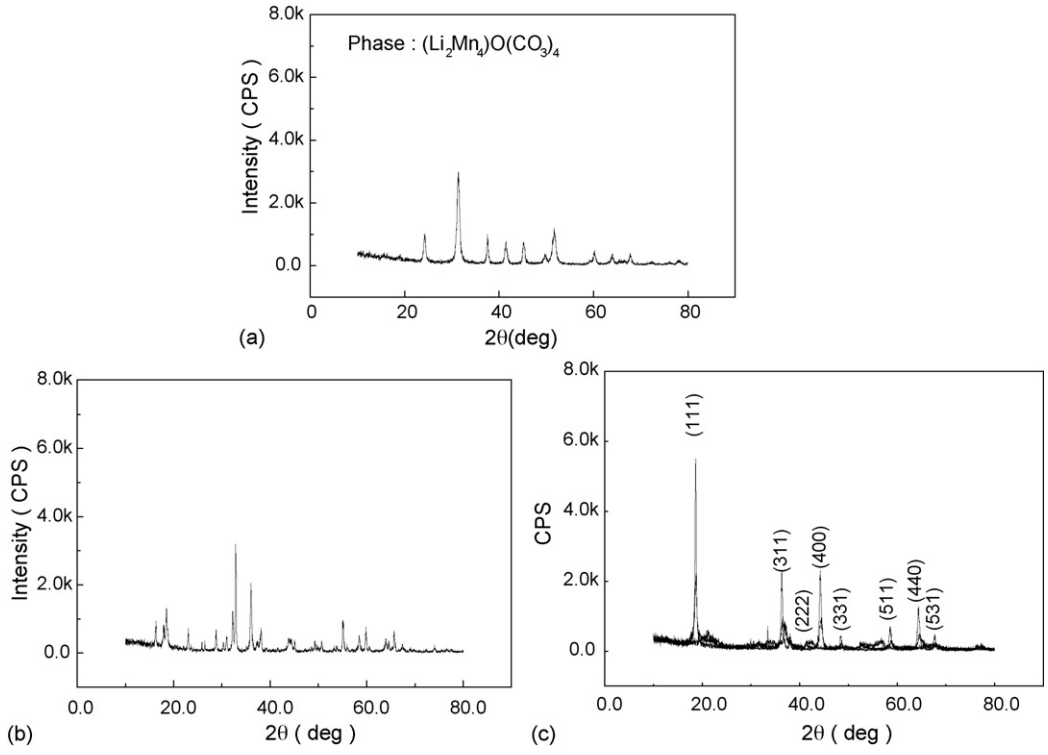

Fig. 2. XRD for precursor during discomposing process: (a) 653 K, (b) 803 K, and (c) 1053 K.

were induced. According to mass action law (7), Arrhenius formula (8), and heating rate formula (9), formula (10) could be deduced.

$$\frac{d\alpha}{dt} = k(1-\alpha)^n \tag{7}$$

$$k = A \ \exp\left(-\frac{E}{RT}\right) \tag{8}$$

$$\beta = \frac{dT}{dt} \tag{9}$$

$$\frac{d\alpha}{dT} = \frac{A}{\beta}e^{-(E/RT)}(1-\alpha)^n \tag{10}$$

where α is the variation, T the temperature, k the reaction velocity constant, n the reaction order number, A the frequency factor, E the active energy, R the gas constant, and β is the heating rate.

In this paper, these four formulas were basic principles. In accordance with Doyle–Ozawa method, the plot of $\log\beta \sim 1/T$ is a line and the slope is $-0.4567E/R$ [10]. In terms of Kissinger principle [11], the formula describing the relation of β, T and E can be written as, $d[\ln(\beta/T_m^2)]/d(1/T_m) = -(E/R)$, where T_m is the maximum temperature of the peak.

Suppose that the reaction velocity was maximum at peak temperature and the reaction was ruled by dynamics equations of Kissinger [12],

$$\frac{d}{dt}\left(\frac{da}{dt}\right) = 0 \tag{11}$$

Formula (11) was substituted into the formula (10), we get

$$\frac{E}{RT_m^2} = \frac{An}{\beta}(1-\alpha_{max})^{n-1} \ \exp\left(-\frac{E}{RT_{max}}\right) \tag{12}$$

For $n = 1$, then

$$\frac{E}{RT_{max}^2} = \frac{A}{\beta} \ \exp\left(-\frac{E}{RT_{max}}\right) \tag{13}$$

For $n \neq 0$ and $n \neq 1$, the approximated formula (14) could be obtained

$$n(1-\alpha_{max})^{n-1} \approx 1 + (n-1)\left(\frac{2RT_{max}}{E}\right) \tag{14}$$

Due to $(n-1)(2RT_{max}/E) \leq 1$, (14) becomes

$$n(1-\alpha_{max})^{n-1} \approx 1 \tag{15}$$

Formula (15) was substituted into formula (12), and the same formula (13) could be inferred.

According to the formula (10)–(15), the corresponding dynamic constants could be calculated.

3.3. Decomposition active energies of precursor for lithium manganese oxide

By means of Doyle–Ozawa method and Kissinger method, we studied the decomposition reaction dynamics of precursor for lithium manganese oxide according to the measured DTA curves. Using Doyle–Ozawa method, the diagrams of $\log\beta \sim 1/T$ for four peaks were showed in the Fig. 3, in which every line expressed percent conversion of 10–100% from the right to the left.

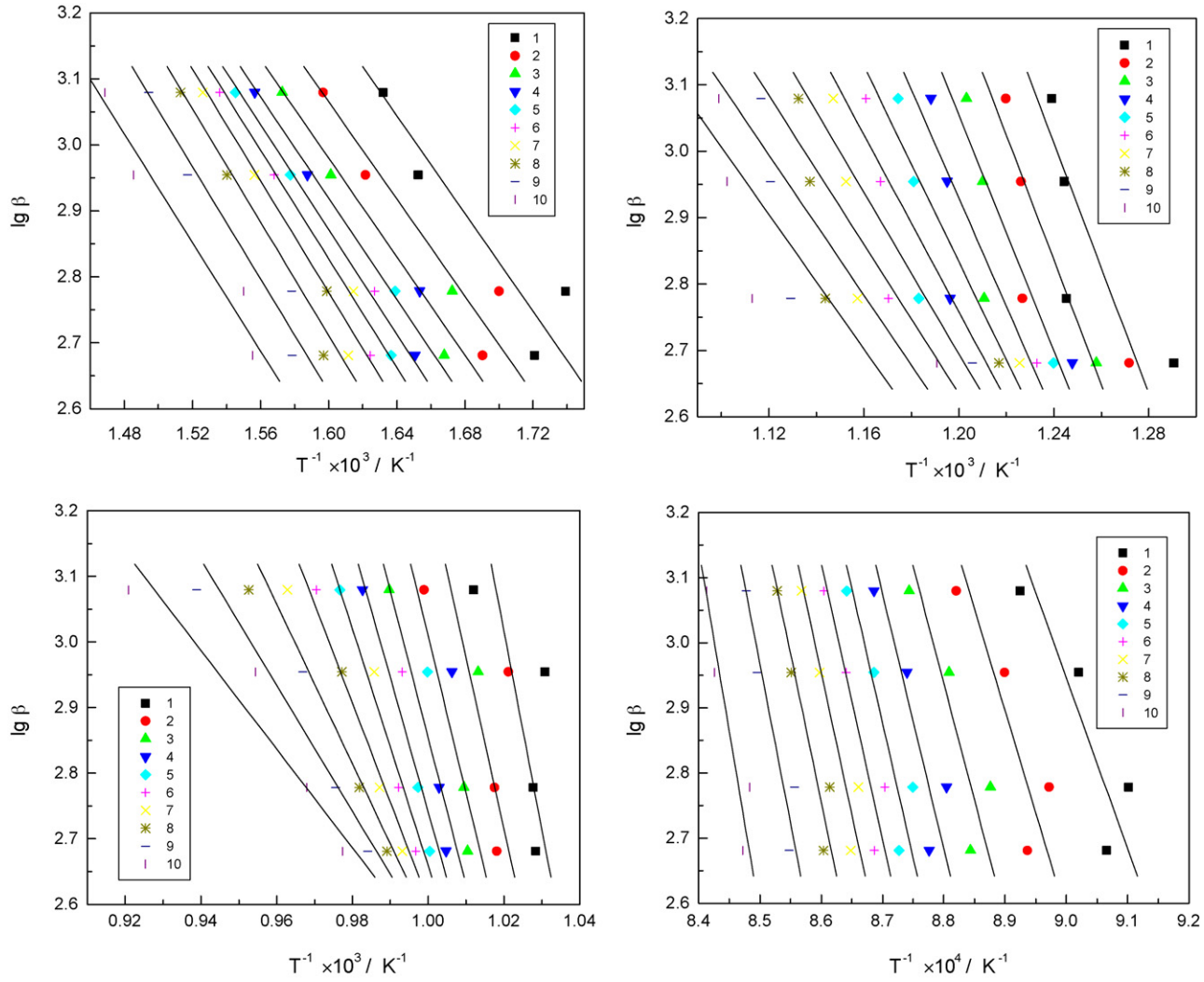

Fig. 3. Active energy of discomposing reactions for the precursors with Doyle–Ozawa method (every line regressed by calculating point of 1–10 symbol expresses reaction degree of 10–100% from the right to the left in each picture).

It could be inferred from Table 1 that the reaction active energy was different for different conversion during the process of the first endothermic peak. And the process could be divided into three stages: 67.537–69.904 kJ mol^{-1}, 69.904–78.198 kJ mol^{-1} and 78.198–74.876 kJ mol^{-1}. Then the average apparent active energy was 72.759 kJ mol^{-1}. Similarly, for the second endothermic peak, the average active energy was decreasing with the conversion increasing, which was from 171.887 kJ mol^{-1} to 92.301 kJ mol^{-1}, and the average active energy was 131.023 kJ mol^{-1}. The same as the third endothermic peak, then the average active energy is 337.877 kJ mol^{-1}. Seemly, the exothermic peak was composed of three

Table 1
Active energy and linear coefficients of each reaction degree at the different peaks E (kJ mol^{-1})

Reaction degree, α (%)	E_1	r_1	E_2	r_2	E_3	r_3	E_4	r_4
10	67.537	−0.924	171.887	−0.785	550.817	−0.680	477.633	−0.885
20	67.037	−0.951	170.999	−0.791	473.952	−0.675	571.050	−0.874
30	67.991	−0.964	161.746	−0.793	436.141	−0.688	652.608	−0.876
40	69.904	−0.969	148.402	−0.793	407.533	−0.719	713.343	−0.889
50	72.378	−0.970	134.331	−0.793	373.501	−0.768	751.849	−0.908
60	74.993	−0.969	121.469	−0.792	328.068	−0.827	774.990	−0.927
70	77.151	−0.969	110.693	−0.793	275.076	−0.882	794.714	−0.941
80	78.198	−0.970	102.261	−0.796	221.817	−0.922	826.351	−0.946
90	77.529	−0.973	96.142	−0.800	174.858	−0.945	890.109	−0.943
100	74.876	−0.974	92.301	−0.807	137.010	−0.956	1022.266	−0.926

Table 2
Peak temperature T_m, active energy E, reaction order n and frequency factor A at different heating rates

No.	β (K min^{-1})	8	10	15	20	Average	E (kJ mol^{-1})	r
First peak	T_m (K)	616.957	616.528	636.369	652.031			
	n	1.040	1.092	1.106	0.984	1.055	66.902	−0.960
	A ($\times 10^{-3}$)	1.302	1.644	1.541	1.445	1.483		
Second peak	T_m (K)	810.844	820.533	826.639	826.556			
	n	0.900	1.706	1.487	1.509	1.401	199.163	−0.949
	A ($\times 10^{-10}$)	3.289	2.832	3.374	4.513	3.502		
Third peak	T_m (K)	1007.409	1003.410	992.464	1024.649			
	n	0.972	1.063	1.653	1.179	1.217	314.379	−0.906
	A ($\times 10^{-14}$)	0.9942	1.455	3.380	1.278	1.777		
Fourth peak	T_m (K)	1158.527	1153.668	1166.803	1168.195			
	n	0.724	0.872	0.724	0.863	0.795	544.476	−0.839
	A ($\times 10^{-22}$)	2.307	3.690	2.856	3.553	3.101		

stages: 477.633–652.608 kJ mol^{-1}, 652.608–826.351 kJ mol^{-1}, 826.351–1022.266 kJ mol^{-1}and the average active energy was 747.491 kJ mol^{-1}.

According to Kissinger method, the active energy was computed with the slope $-(E/R)$ of the line, which meant plotting a line for $\ln(\beta/T_m^2)$ versus $1/T_m$. The shape factor was calculated beginning temperature, ending temperature and the peak temperature, from which the reaction order was deduced. The frequency factor was obtained according to the formula (12). The kinetic coefficients were listed in Table 2.

The average reaction active energy of each peak was computed with Doyle–Ozawa method and Kissinger method, respectively. The data were given in Table 3.

The reaction mechanism was assured after obtained dynamics parameters in terms of unequal isothermal process. It could be considered that an unequal isotherm process was as an isothermal process within infinite time intervals by Satanva [13]. So, the reaction velocity could replace the general formula during the isotherm process. In accordance with formula (10), Tables 2 and 3, the velocity equations of each peak were as follows:

$$\frac{d\alpha}{dt} = 1.483 \times 10^3 e^{-(69831/RT)}(1-\alpha)^{1.055},$$

$$\frac{d\alpha}{dt} = 3.502 \times 10^{10} e^{-(165093/RT)}(1-\alpha)^{1.401}$$

$$\frac{d\alpha}{dt} = 1.777 \times 10^{14} e^{-(326128/RT)}(1-\alpha)^{1.217},$$

$$\frac{d\alpha}{dt} = 3.101 \times 10^{22} e^{-(645983/RT)}(1-\alpha)^{0.795}$$

Table 3
Active energies of each peak using

Method	E_1	E_2	E_3	E_4
Doyle–Ozawa	72.759	131.023	337.878	747.491
Kissinger	66.902	199.163	314.379	544.476
Average	69.831	165.093	326.128	645.983

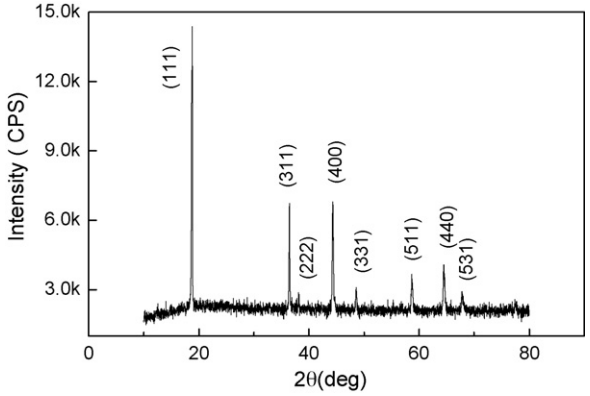

Fig. 4. X-ray diffraction pattern of $LiMn_2O_4$.

3.4. Phase and microstructure results

According to the differential thermal analysis experiments and kinetics calculations, we designed the orthogonal experiments of two factors (including sintering temperature and thermostat time) and three levels during the sintering course

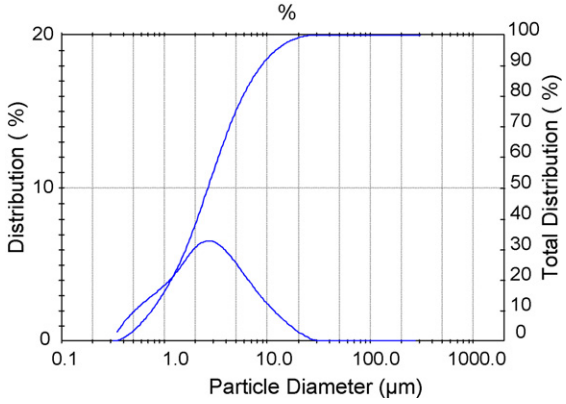

Fig. 5. Granularity analysis of $LiMn_2O_4$.

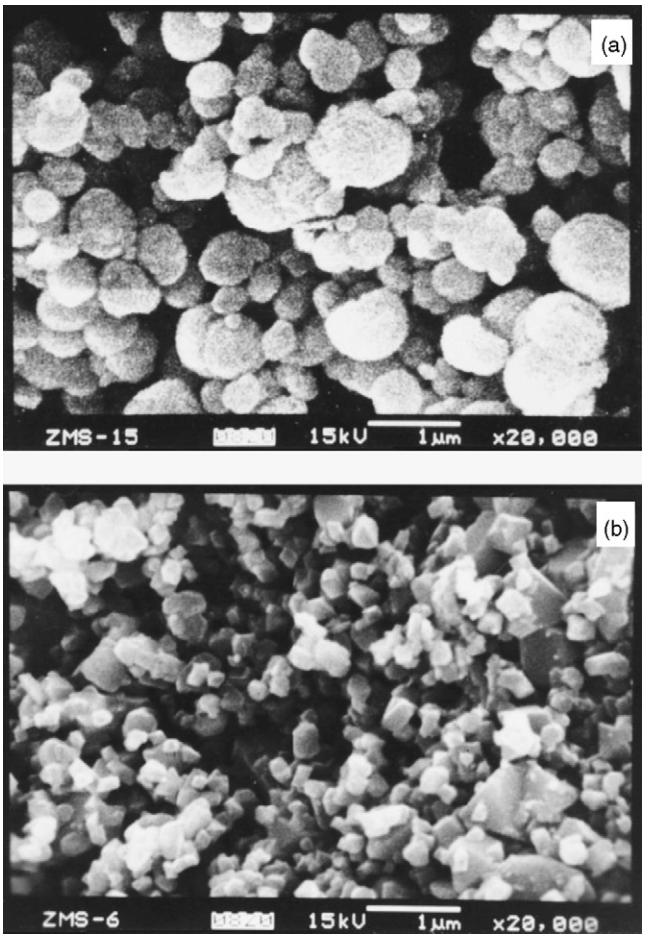

Fig. 6. SEM photos of the precursor and $LiMn_2O_4$. (a: precursor and b: lithium manganese oxide).

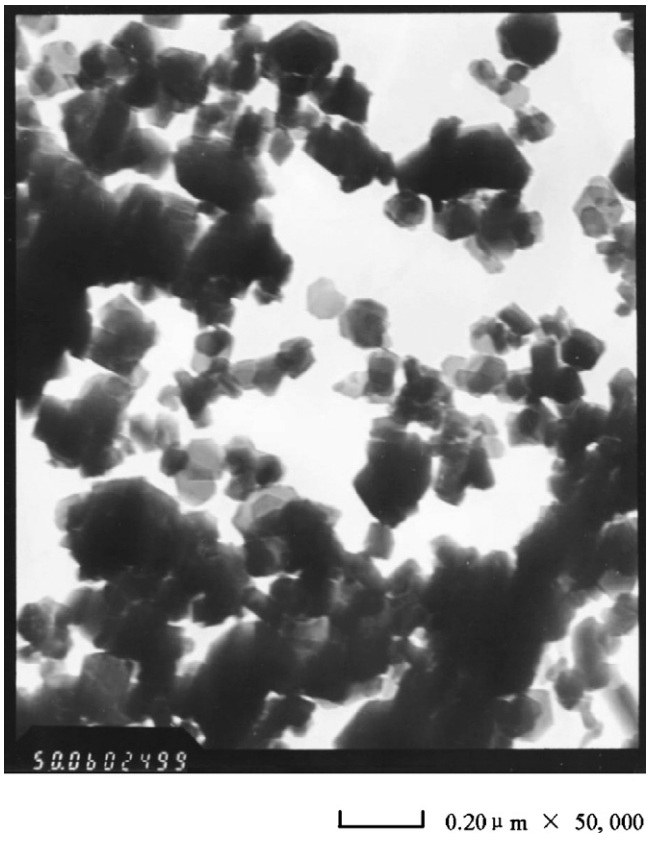

Fig. 7. TEM photo of $LiMn_2O_4$.

[14]. Among these experiments, the measurement target was the beginning discharge capacity. After the orthogonal experiments, the optimal experiment conditions were assured that the sintering temperature was 650 °C and the thermostat time was 6 h for the precursor prepared using carbonate co-precipitation method. Then, lithium manganese oxide with spinel structure was prepared using carbonate co-precipitation method and sintering method. XRD, particle distribution, SEM and TEM of the sample were showed in Figs. 4–7, respectively. From Fig. 4, the crystal development of $LiMn_2O_4$ was superior and unpurified phase was few. Especially, the crystallinity of crystal face (1 1 1), (3 1 1), (4 0 0) was rather high. It could be seen from Fig. 5 that distribution of particle size was normal, and the average granularity was 2.57 μm. The particles were well distributed and the appearance was regular without obvious conglomeration from Fig. 6. Fig. 7 indicated that the crystal grew completely and the individual size could reach to nano level. All the kinetic results could optimize the reaction condition and the high quality of spinel $LiMn_2O_4$ sample could be prepared, which meant the ratio surface was large, thus, the product has good chemical activity and its discharge–capacity ratio was well.

4. Conclusion

There are two endothermic peaks and two exothermic peaks existed during the decomposition process of lithium manganese oxide precursor at dynamic air atmosphere under four different heating rates of 8, 10, 15 and 20 K min^{-1}. Using DTA and XRD measurements, decomposition process of lithium manganese oxide precursor could be divided into three stages of dehydration, decomposition and synthesis. The apparent active energies of four peaks are calculated with Doyle–Ozawa method and Kissinger method. The average values are 69.831, 165.093, 326.128, 645.983 kJ mol^{-1}, respectively. Using Kissinger method the peak shape index, reaction order number and the temperature range were obtained, then the dynamic velocity equations were deduced. On the basis of DTA experiments and kinetics calculations, lithium manganese oxide was prepared using carbonate co-precipitation method and sintering method, and the result is a pure phase, well-distributed particle and has regular appearance with spinel structure.

Acknowledgements

This work was financially supported by the China postdoctoral science fund (No. 0200360009) and Xi'an Jiaotong University introduced talents fund (No. 090071181).

References

[1] J.R. Dahn, V.U. Sacker, M.W. Juskow, H.A. Janaby, J. Electrochem. Soc. 138 (1991) 2207.
[2] G. Pistonia, A. Antonini, D. Zane, Solid State Ionics 78 (1995) 115.
[3] H.X. Li, Battery World 2 (1999) 26.
[4] H.X. Li, Battery World 2 (2000) 34.
[5] J.M. Tarascon, W.R. Mckinnon, T.N. Bowmer, et al., J. Electrochem. Soc. 141 (1994) 1421.
[6] Y.S. Lee, Y.K. Sun, K.S. Nahm, Solid Ionic State 109 (1998) 285.
[7] Ming-shu Zhao, Yu-chun Zhai, Yan-wen Tian, et al., Chin. J. Power Sources 25 (2001) 246.
[8] H.B.T.L. Shen, Thermal Analyses (translated by Z.H. Liu, Beijing), Chemistry Industry Publishing House, 1992, pp. 1–14.
[9] X. Shen, Differential Thermal or Thermogravimetry Analyses and Dynamic for Non-isotemperature Solid Phase Reaction Process, Metallurgy Industry Publishing House, Beijing, 1995, pp. 22–25.
[10] Z.Q. Cai, Thermal Analyses, Higher Education Publishing House, Beijing, 1993, pp. 68–73.
[11] B.L. Yu, J.D. Jiang, Practical Thermal Analyses, Beijing Textile Industry Publishing House, 1990, p. 54, 151, 168, 208.
[12] Z.R. Hu, Q.Z. Shi, Thermal-Analyses Kinetics, Beijing Science publishing house, 2001, p. 109, 110.
[13] H. Zhou, W.M. Zeng, Chin. J. Nonferr. Metals 3 (1993) 40.
[14] Ming-shu Zhao, Researches and Preparations of Spinel $LiMn_2O_4$ and Correlated Materials for Lithium-ion Batteries Cathode, Ph.D. Dissertation, Northeastern University, 2002, pp. 136–141.